Electron microscopy study of CeO$_x$−Pd/α-Al$_2$O$_3$ catalysts for methane dry reforming

M. S. Moreno,[1,a)] F. Wang,[2] M. Malac,[2] T. Kasama,[3] C. E. Gigola,[4] I. Costilla,[4] and M. D. Sánchez[4,5]

[1]*Centro Atómico Bariloche, Bustillo 9500, 8400 San Carlos de Bariloche, Argentina*
[2]*National Institute for Nanotechnology, Edmonton T6G 2M9, Canada*
[3]*Department of Materials Science and Metallurgy, University of Cambridge, Cambridge CB2 3QZ, United Kingdom*
[4]*Planta Piloto de Ingeniería Química, La Carrindanga km 7, 8000 Bahía Blanca, Argentina*
[5]*Departamento de Física, Universidad Nacional del Sur, 8000 Bahía Blanca, Argentina*

We have investigated the interaction between Pd and Ce in a (0.47 wt %) CeO$_x$−Pd(1 wt %)/α-Al$_2$O$_3$ catalyst that is used in the reforming reaction of CH$_4$ with CO$_2$. The freshly reduced catalyst was characterized by various electron microscopy techniques, such as elemental mapping, Z-contrast imaging, and electron energy-loss spectroscopy to understand the role of Ce on a microscopic scale. The high spatial resolution elemental mapping indicates that CeO$_x$ is located in close proximity of the palladium nanoparticles. High-resolution lattice images and energy-loss spectra obtained in the vicinity of the Pd particles show an anisotropic distribution of CeO$_x$ crystallites limited to the interface region between Pd and the substrate but not covering the surface of the Pd nanoparticles. Energy-loss near edge fine structure of Pd M edges reveals that the Pd nanoparticles are not oxidized. © *2009 American Institute of Physics.* [DOI: 10.1063/1.3115405]

I. INTRODUCTION

The reforming reaction of CH$_4$ with CO$_2$ has motivated numerous studies in search of active and selective catalysts, considering the existence of significant natural gas deposits with high CO$_2$ content that could be used to produce synthesis (CO+H$_2$) gas. The overall reaction scheme can be represented by the following reactions:

$$CH_4 \leftrightarrow C + 2H_2,$$

$$CO_2 + C \leftrightarrow 2CO.$$
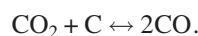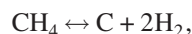
The endothermic character of this reaction requires a high reaction temperature to obtain acceptable conversion levels. The high operating temperature puts stringent requirement on suitable catalysts. Often the high temperature results in sintering of metallic particles and deactivation of the catalyst by the formation and accumulation of carbonaceous deposits.[1]

It was demonstrated that supported noble metal catalysts[2–4] are active and selective for the dry reforming reaction, but the high cost limits their practical applications, making desirable to find alternative. Ni and Pd can be used for reforming with CO$_2$ providing special support or adding promoters like LaO$_3$, CaO, and CeO$_2$ that prevent or reduce the carbonaceous deposit formation. In the case of CeO$_2$, the reaction scheme can be described as follows:
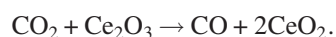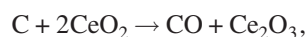
$$C + 2CeO_2 \rightarrow CO + Ce_2O_3,$$

$$CO_2 + Ce_2O_3 \rightarrow CO + 2CeO_2.$$

The use of Pd as an active metal is particularly attractive due to its remarkable activity for the decomposition of CH$_4$ (Ref. 5) at high temperature, favoring the production of H$_2$ and the formation of carbonaceous deposits. Nagaoka and Aika[1] showed that the use of CeO$_x$ (where the mass fraction of Ce is five times higher than Pd) in a Pd(2 wt %)/γ-Al$_2$O$_3$ catalyst at 1023 K reduces the formation of carbonaceous deposits. We have recently shown[6] that the addition of 2.5 wt % of Ce to a Pd(1 wt %)/α-Al$_2$O$_3$ catalyst practically eliminates the carbonaceous deposits, with a slight increase in the resulting CO/H$_2$ ratio. In this case, a slow diminution of the activity level converging to a constant, nonzero, activity was observed. Following our previous studies we have recently investigated the effect of Ce loading in detail, having verified that it can be reduced to below Pd content, without altering its capacity to inhibit the carbonaceous deposit formation. The deactivation (defined as 1-[(CH$_4$ conversion at time $t>0$)/(CH$_4$ conversion at time $t=0$)]) of a Pd(1%)/α-Al$_2$O$_3$ used for the reforming of CH$_4$ with CO$_2$ at 923 K decreased from 72% to 14% in 35 h, after the addition of 0.47 wt % of Ce (Ref. 7). The remaining deactivation was due to the sintering of the Pd particles. Our previous results on bulk samples also showed, by means of x-ray photoelectron spectroscopy (XPS), that on average Ce is present in several oxidation states and that for a similar fresh sample (Ce 0.33 wt %), with an average particle size below 15 nm, the binding energy of Pd does not reach the value of reference for metal Pd by less than 1 eV. This shift in average binding energy of Pd is not observed when Ce is not present in the sample. Consequently it indicates the existence of a Pd–Ce interaction averaged over a bulk sample.

In order to understand the role of Ce in the reforming reaction, it is necessary to examine how it interacts with the

---

a)Author to whom correspondence should be addressed. Electronic mail: smoreno@cab.cnea.gov.ar.

Pd particles on a microscopic scale. Average values can be obtained using techniques such as x-ray diffraction (XRD), temperature programmed reduction and desorption (TPR-TPD), and XPS spectroscopy, which provide only indirect or *averaged* information on aspects such as Ce location and proximity to Pd and Pd oxidation state. It is worth noting that XPS provides surface sensitive results. Transmission electron microscopy (TEM) provides information easily down to nanometer scale, but the use of electron microscopy on Ce–Pd interaction has been far less extensive. An article by Holles *et al.*[8] reported the use of high-resolution TEM and the observation of small ceria crystallites of about 3 nm average size dispersed over the alumina support. Their work was performed on Pd-Ce/γ-Al$_2$O$_3$ catalysts with high Ce loadings (5–30 wt %), indicating that Ce could be located either around and/or over the Pd particles. However, the examinations of Ce oxide phases in samples with low Ce concentrations require techniques that allow a *direct visualization* of the Ce distribution and a local study of the initial Pd oxidation state. Here, we report a TEM investigation of a CeO$_x$(0.47%)$-$Pd(1%)/α-Al$_2$O$_3$ catalyst, revealing direct information on both the elemental distributions, the relative location of CeO$_x$ and Pd, and the oxidation state of Pd on a *microscopic* scale with bulk elemental sensitivity.

II. EXPERIMENTAL

A supported Pd catalyst with 1 wt % Pd metallic content was prepared by successive impregnation of α-Al$_2$O$_3$ (Rhone Poulenc; $S_g = 10$ m^2/g) with a solution of Pd acetyl acetonate in toluene (3.0×10^{-3} g Pd/ml). The support was kept in contact with the solution for 24 h, then filtered, dried in flow of nitrogen gas, and calcined in chromatographic air at 773 K for 1 h. The preparation was then reduced with pure H$_2$ at 573 K. The CeO$_x$$-$Pd/$\alpha$-Al$_2O_3$ catalyst was obtained by impregnation of the above Pd/α-Al$_2$O$_3$ with an aqueous solution of Ce(NH$_4$)$_2$(NO$_3$)$_6$. After a drying step the preparation was calcined in chromatographic air at 1009 K, reduced in pure H$_2$ at 573 K, cooled to room temperature, and exposed to atmospheric air. The fraction of exposed Pd atoms measured by H$_2$ chemisorption using the double isotherm method was 0.14, and the amount of Ce incorporated in the sample, as determined by inductive coupling plasma, was 0.47 wt %.

The activity and selectivity of the catalyst were determined in a flow reactor operated at 1300 Torr and 923 K, which was fed with a CH$_4$/CO$_2$/Ar (25/25/50 mol %) mixture. A catalyst load of 400 mg diluted with an equal amount of α-Al$_2$O$_3$ was placed at the center of a quartz tube (4 mm internal diameter and 80 mm length) in a Lindberg-Blue M electric furnace with three independent heating zones. Using a total flow of 200 ml/min, the gas hourly space velocity was 23 250 h^{-1}. The reaction temperature was monitored by a thermocouple located at one end of the catalysis bed. Before the reaction, the catalyst was reduced at room temperature with a H$_2$(5%)/Ar mixture, with subsequent temperature elevation up to 923 K in Ar. Reactants and products were analyzed by gas chromatography (GC) using two on line instruments with thermal conductivity detectors. In one of

the GCs a silica gel column (6 ft x 8 in.) at 363 K with He as carrier was used to separate CO$_2$. In another unit, the content of H$_2$, CO, and CH$_4$ was analyzed using a Chromosorb 102 column (14 ft x 1/8 in.) with Ar flow. The water formed by the reverse water gas shift (RWGS) reaction CO$_2$ +H$_2$$\leftrightarrow$CO+H$_2$O was separated by a silica gel bed. The H$_2$O concentration in the outflow stream was estimated from the O$_2$ balance.

Specimens for electron microscopy studies were prepared by ultrasonically dispersing the catalyst powder in alcohol and placing the dispersion onto a holey carbon-coated copper grid. A Tecnai F20 (G^2) was used for elemental mapping, and a JEOL 2200 FS microscope was used for Z-contrast imaging, parallel nanobeam diffraction, and electron energy-loss spectroscopy (EELS). Both microscopes were operated at 200 kV, and the samples were examined at room temperature. Parallel nanobeam diffraction (NBD) using a sub-30 nm probe was done by operating the microscope in free lens control. Elemental mapping for Ce was done using the three-window background-subtraction method.[9] An objective aperture defining a collection semiangle of $\sim$4 mrad was used to provide a close-to-optimal spatial resolution for energy-filtered imaging. Three energy-loss images were acquired using an energy window width of 30 eV, one just above the 883 eV onset of the Ce $M_{4,5}$ edge (centered at 898 eV) and two below the edge (at 828 and 858 eV). For EELS measurements, a focused beam with 0.5 nm diameter was used. The energy resolution of the energy-loss spectrum (as defined by the full width at half maximum (FWHM) of the zero-loss peak) was about 1 eV. Since a Z-contrast image is formed by detecting the electrons that have suffered Rutherford scattering, the intensity is approximately proportional to Z^2. For the catalyst under study this means that the image contrast is highly sensitive to the presence of Pd and Ce (high Z) particles or clusters.

III. RESULTS AND DISCUSSION

In Fig. 1(a) the conversion of CH$_4$ and CO$_2$ as a function of time is compared for a monometallic catalyst Pd(1 wt %)/α-Al$_2$O$_3$ and a modified one fed with a CH$_4$/CO$_2$/Ar (25/24/50) mixture. The effect of the addition of a small amount of Ce on the Pd/α-Al$_2$O$_3$ catalyst stability can be clearly appreciated. The CO$_2$ conversion is greater than the CH$_4$ one due to the RWGS reaction, which consumes H$_2$ and generates CO and H$_2$O. Therefore, the CO/H$_2$ relation in the outflow stream was 1.3. The diminution in the activity of the catalyst after 35 h reaction is due to the sintering process of the metal particles.[7] The noticeable deactivation of the monometallic catalyst after 20 h is attributed to the carbon nanofiber formation on the Pd particle surface.[10] This effect is also demonstrated by the significant drop in the H$_2$ selectivity of about 6% between 20 and 25 h reaction, as shown in Fig. 1(b). While the monometallic catalyst was initially $\sim$3% more selective than the one with Ce content, the selectivity of the latter remains approximately constant during the 35 h of reaction with a selectivity loss of about 1% over the 35 h period. The difference in the initial selec-
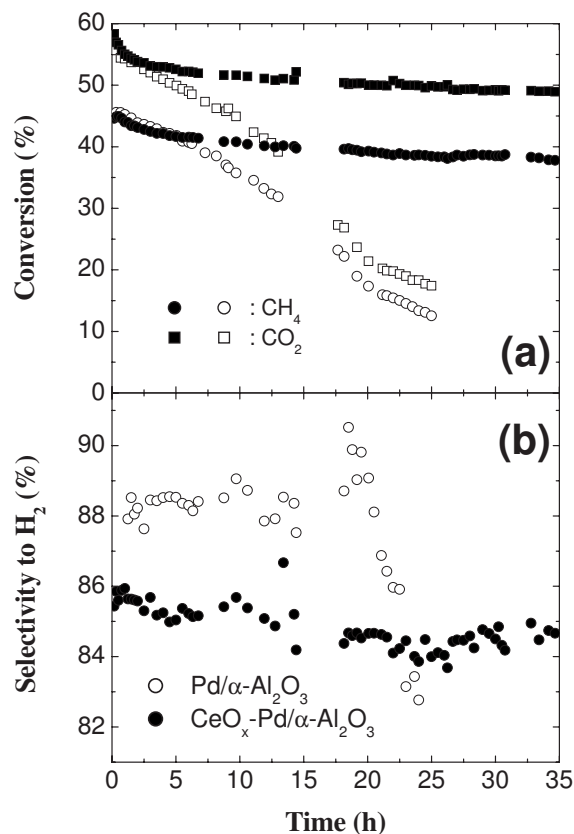
FIG. 1. Effect of Ce addition on the CH_4 and CO_2 conversion for Pd(1 wt %)/α-Al_2O_3 (open symbols) and CeO_x–Pd/α-Al_2O_3 (filled symbols) (a). H_2 selectivity as a function of reaction time for both catalysts, monometallic and modified (b).

tivity may be derived from the reduction in active sites as a result of the metal particle size growth during the catalyst preparing process.[6]

The location of Ce in the proximity of the Pd nanoparticles could explain the inhibition of carbonaceous deposit formation using this promoter. As mentioned above, the well known redox capability of Ce contributes to oxidization of C, thus maintaining the catalyst activity. Therefore, understanding the role of Ce in the reforming reaction and the inhibition of carbonaceous deposits is related to measurements that provide direct information on their spatial distribution and electronic structure of Pd.

Figure 2 shows a representative Z-contrast image of the sample and the corresponding Pd particle size distribution. The image clearly shows that many small Pd particles, seen
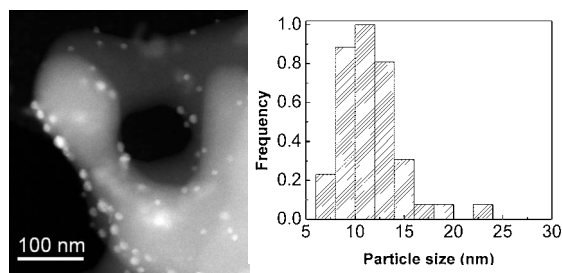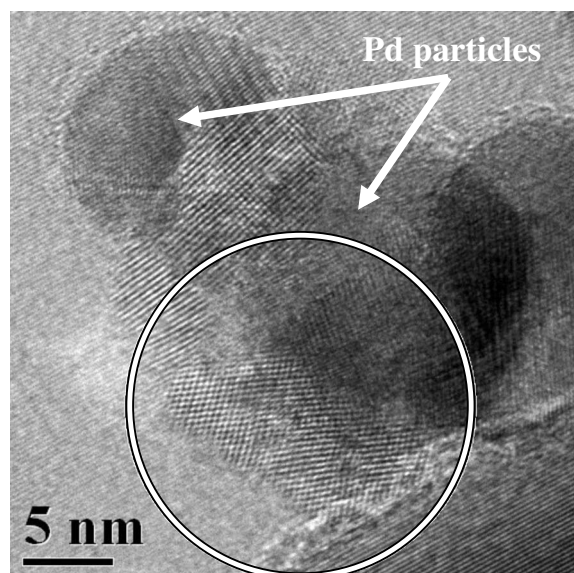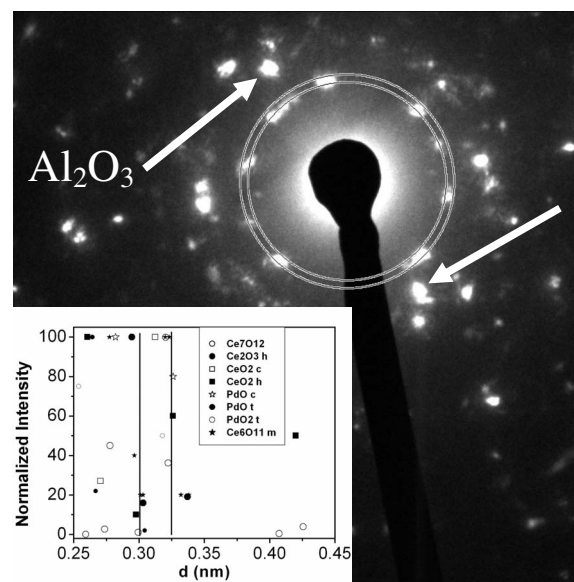

FIG. 2. Low magnification high angle annular dark field (Z-contrast) image of the catalyst (left) obtained in scanning transmission mode of a TEM. Particle size distribution of Pd nanoparticles (right).

FIG. 3. (a) Image of the catalyst. The Pd particles are marked with arrows. The small crystals close to Pd particles correspond to the Ce oxide phases. The circle indicates the region analyzed by diffraction in (b). NBD pattern of the region marked in a). The circles correspond to spacings in real spaces of 0.3 and 0.325 nm. The inset shows all the possible phases and their spacings. White arrows indicate the reflections of Al_2O_3 used as internal standard.

as bright features, are formed. The particle size distribution shows that the major fraction of the particles has a diameter below 15 nm. Only a few particles larger than 16 nm were observed.

Figure 3(a) shows an image of the catalyst. The Pd particles are seen as the darker rounded features in the image (marked with an arrow). A second interesting feature is the presence of small crystals close to the Pd particles. Because of their random orientations, most of particles show lattice fringes only in one direction. Typical *d*-spacings measured from the power spectrum fast Fourier transform (FFT) of the lattice fringes fall in the range 0.27–0.33 nm. This procedure
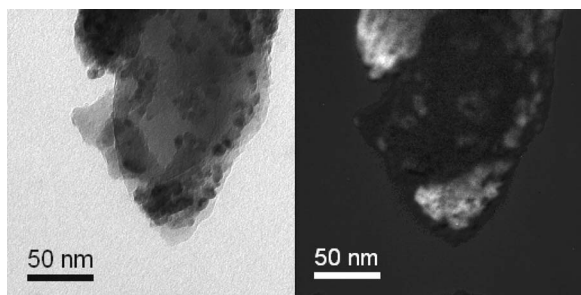
FIG. 4. Zero-loss filtered image (left) and the corresponding Ce elemental map (right).

FIG. 5. Z-contrast image showing the positions of the EEL spectra acquired from a Pd particle, surface (s), center (c), and interface (i).

provides reliable average lattice spacings in tilted particles as opposed to the examination of distances between individual lattice planes in high-resolution images which can give smaller or bigger values than the real one.[11] These values are clearly different from the maximum lattice spacing of ~0.24 nm for $CePd_3$ and $CePd_5$ alloys or metallic Pd.[12] Diffraction techniques often provide more reliable measurement of lattice spacings than imaging and provide measurable Bragg reflections far beyond the information limit of a TEM. Figure 3(b) shows a NBD pattern recorded from the area labeled by the circle in Fig. 3(a). In the inset are shown all the phases that can be found in this system. The two circles in the NBD pattern confirm a range of spacings which cannot be attributed to other phases than PdO_x or CeO_x phases. As we will show below, the presence of PdO_x phases can be ruled out. A precise phase identification of these CeO_x crystals is difficult because of several factors. (i) The orientation is such that only one set of lattice fringe spacings is frequently observed. (ii) The lack of the large lattice spacings (higher than 0.33 nm) does not allow us to assign these phases unambiguously, although a careful measurement of these images suggests that the small crystals likely correspond to some CeO_x phases, such as Ce_2O_3 and intermediate phases, Ce_6O_{11} and/or Ce_7O_{12}. The existence of intermediate phases is thermodynamically feasible[13,14] under the present thermal treatment conditions and their presence is in agreement with previous XPS results[7] that confirmed the presence of Ce in several oxidation states. It should be noted that the small crystals are anisotropically distributed around the Pd particles. Particles located at the edge of the alumina substrate allow to distinguish clearly particle surface and substrate and allow a more accurate assessment of the CeO_x crystallite distribution. We frequently observed that Ce crystallites do not cover the surface of the Pd particle.

A zero-loss filtered image and the corresponding Ce elemental map are shown in Fig. 4. The map clearly shows that Ce is located in the vicinity of Pd particles (seen as the darker regions in the zero-loss filtered image). This finding provides additional support to the observations shown in Fig. 3 and to the implication that the small crystals may be a Ce oxide phase. It should be noted that oxygen mapping does not provide interpretable information because the Al_2O_3 support contains oxygen.

Figure 5 shows a higher magnification Z-contrast image of the sample, in which a Pd particle coexisting with an alumina crystal is clearly observed because of the large dif-
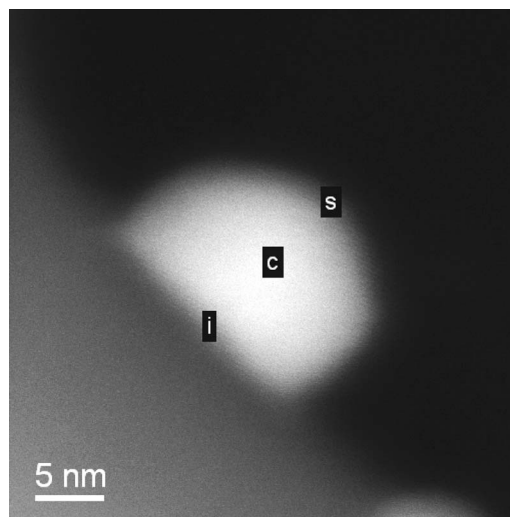
ference between the atomic numbers of Pd and Al and O. Although Ce detection against alumina has the same favorable conditions as Pd we could not detect the small CeO_x crystals around the Pd particle possibly because the Z-contrast difference between Pd and Ce is not sufficient to distinguish Pd from Ce oxides. Energy-loss spectra were acquired from the positions indicated in the image of Fig. 5 in order to determine the local oxidation state of Pd. The background of these spectra was subtracted using standard power law fit,[9] and the spectra are shown without any additional processing. Figure 6(a) shows the EEL spectra acquired from
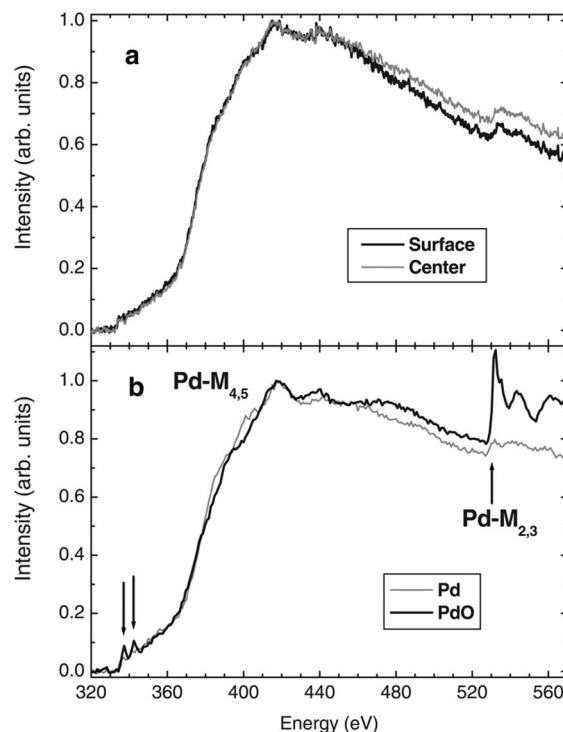

FIG. 6. (a) EEL spectra acquired for a single Pd nanoparticle from the region marked in Fig. 5. (b) Reference spectra for bulk Pd metal and PdO. The Pd $M_{4,5}$ (at 335 eV) and Pd M_3 (~520 eV) edges and the oxygen K edge at 532 eV can be seen.
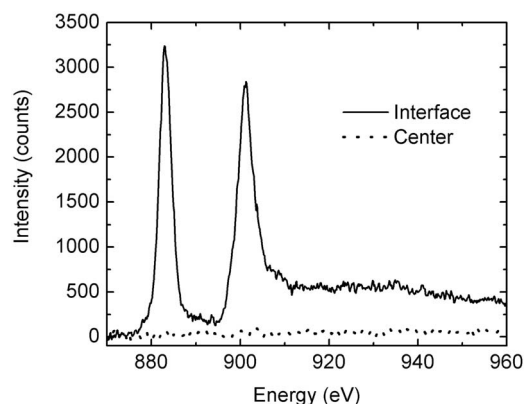
FIG. 7. EEL spectra of Ce $M_{4,5}$ edge acquired from a single Pd nanoparticle from the region marked in Fig. 5.

FIG. 8. Schematic drawing depicting the distribution of CeO_x phases, the reaction scheme, and surface mechanism for CH_4 with CO_2 reforming reaction process over the CeO_x–Pd/α-Al_2O_3 catalyst.

a single Pd nanoparticle, as marked in Fig. 5 at particle surface (s) and center (c). The spectra show the Pd $M_{4,5}$ (at 335 eV) and Pd $M_{2,3}$ ($\sim$520 eV) edges. In Fig. 6(b) are shown reference spectra[15] for metal Pd and PdO. It can be seen that the Pd $M_{2,3}$ follows the $M_{4,5}$ edges of Pd, being completely overlapped with the O K edge (at 532 eV) in the palladium oxide phase.

In order to determine the oxidation state of Pd it is important to identify characteristic features in the spectrum that allows to distinguish between metal Pd and its oxides. It should be noted that the Pd M edges are delayed edges. Consequently there is little difference in the fine structure that allows to distinguish between Pd and PdO phases by analyzing only the Pd $M_{4,5}$ edges. The only difference appears at the edge threshold (marked with an arrow in Fig. 6) where two more pronounced peaks can be seen in PdO, compared to metal Pd, and in the shape of the edge with PdO having a peak at about 395 eV while metal Pd shows two peaks at 385 and 400 eV. These differences are of some help when analyzing data with high signal/noise ratio; its value is frequently of less importance in the analysis of EELS data acquired using a small probe because the signal to noise ratio is lower for this type of data. The region of the spectrum above 520 eV is more useful even though the Pd $M_{2,3}$ overlaps with the O K edge. It should be noted that the delayed nature of the Pd $M_{2,3}$ edge only contributes to an almost structureless background. Any visible fine structure if present should be assigned to oxygen K edge. At the same time, for the oxide phase the intensity above 525 eV has to be appreciably higher than in metal Pd. These two features give an unambiguous identification of the oxidation state even for data with a low signal to noise ratio.

Spectra of Fig. 6(a) were acquired from the surface and the center of the particle. According to the above description these spectra show the features typical for metallic Pd, i.e., the two peaks in the Pd $M_{4,5}$ and the lack of a strong fine structure at the oxygen K edge energy.

Figure 7 shows the Ce $M_{4,5}$ EEL spectra acquired for a single Pd nanoparticle from the region marked in Fig. 5. These spectra were processed as described above. The Ce $M_{4,5}$ edges showing white lines can be observed only for the spectrum acquired at the interface region between the Pd nanoparticle and the substrate. Ce was not detected in other
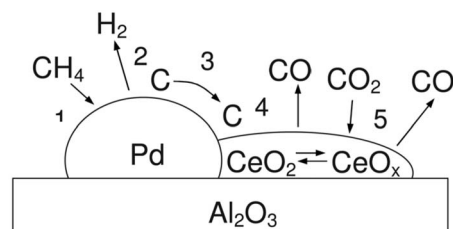
regions than the interfaces. Spectra acquired around the Pd nanoparticles showed a nonuniform distribution of Ce. These two results are in good agreement with our high resolution TEM (HRTEM) and NBD observations, that is, Ce–Pd alloys and/or decoration of Pd particles by Ce oxide particles can be ruled out.

Our results on the distribution of Ce oxides in coexistence with the metallic Pd nanoparticles are summarized schematically in Fig. 8 together with the surface mechanisms for the CH_4 and CO_2 reforming reaction over CeO_x–Pd/α-Al_2O_3. The reaction can be as follows: (1) CH_4 adsorption, (2) CH_4 dissociation, (3) C surface diffusion, (4) C oxidation and CeO_2 reduction, and (5) CO_2 reduction and CeO_x oxidation.

The preceding results exclude the presence of Pd in an oxidized state. We have not observed a chemical shift of the Pd edges across the particles. This result is not in contradiction with our previous XPS measurements that showed a shift of less than 1 eV in the binding energy of Pd. EELS chemical shifts are complicated phenomena[16] involving two qualitatively different orbitals: the core level and the lowest energy occupied level. This makes them sensitive to the sample band structure, and a full explanation would involve full electronic structure calculations which are beyond the scope of this work. The metallic character of the Pd nanoparticle may suggest that an electronic mechanism like charge exchange with the CeO_x crystals might be responsible for the shift observed by XPS.

IV. CONCLUSIONS

A combination of several TEM techniques has been used to study and determine the structure of a CeO_x–Pd/α-Al_2O_3 catalyst at high spatial resolution. Our results clearly demonstrate that the Pd nanoparticles, reduced and exposed to air, are not oxidized. The CeO_x species distributes at the Pd-substrate interface but does not cover the surfaces. High-resolution images and NBD suggest the presence of more than one CeO_x phase. This means that a coexistence of different Ce oxidation states should take place. This is in agreement with our XPS results reported in a previous study.[7] This Pd–CeO_x interaction facilitates the participation of a redox process that prevents the accumulation of C during the reforming reaction. The well known reducibility of Ce^{4+} to Ce^{3+} contributes to C elimination by CO formation while the dissociation of CO_2 on Ce^{3+} species helps to recover the highest oxidation state of cerium.

ACKNOWLEDGMENTS

[1] K. Nagaoka and K. Aika, Bull. Chem. Soc. Jpn. **74**, 1841 (2001).

[2] J. H. Bitter, K. Seshan, and J. A. Lercher, J. Catal. **171**, 279 (1997).

[3] A. Erdohelyi, A. Cserenyi, and F. Solymosi, J. Catal. **141**, 287 (1993).

[4] H. Y. Wang and E. Ruckenstein, Appl. Catal., A **204**, 143 (2000).

[5] J. R. Rostrup-Nielsen and J. Bak-Hansen, J. Catal. **144**, 38 (1993).

[6] P. G. Schulz, M. G. Gonzalez, C. E. Quincoces, and C. E. Gigola, Ind. Eng. Chem. Res. **44**, 9020 (2005).

[7] C. E. Gigola, M. S. Moreno, I. Costilla, and M. D. Sánchez, Appl. Surf. Sci. **254**, 325 (2007).

[8] J. P. Holles, R. J. Davis, T. M. Murray, and J. M. Howe, J. Catal. **195**, 193 (2000).

[9] R. F. Egerton, *Electron Energy Loss Spectroscopy in the Electron Microscope*, 2nd ed. (Plenum, New York, 1996).

[10] M. D. Sánchez, M. S. Moreno, I. Costilla, and C. E. Gigola, Catal. Today **133–135**, 842 (2008).

[11] J.-O. Malm and M. O'Keefe, Ultramicroscopy **13**, 68 (1997).

[12] ICDD Card Nos. 17-0023 and 51-0638.

[13] E. A. Kümmerle and G. Heger, J. Solid State Chem. **147**, 485 (1999).

[14] M. Zinkevich, D. Djurovic, and F. Aldinger, Solid State Ionics **177**, 989 (2006).

[15] C. C. Ahn and L. L. Krivanek, *EELS Atlas* (ASU Center for Solid State Science, Tempe, AZ/Gatan Inc., Warrendale, PA, 1983).

[16] R. Brydson, EMSA Bull. **21**, 57 (1991).